Quantum Trajectory Dynamics in Arbitrary Coordinates†

Vitaly A. Rassolov,‡ Sophya Garashchuk,*,‡,§ and George C. Schatz§

Department of Chemistry and Biochemistry, University of South Carolina, Columbia, South Carolina 29208, and Department of Chemistry, Northwestern University, Evanston, Illinois 60208-3113

Received: November 21, 2005; In Final Form: January 19, 2006

The quantum trajectory approach is generalized to arbitrary coordinate systems, including curvilinear coordinates. This allows one to perform an approximate quantum trajectory propagation, which scales favorably with system size, in the same framework as standard quantum wave packet dynamics. The trajectory formulation is implemented in Jacobi coordinates for a nonrotating triatomic molecule. Wave packet reaction probabilities are computed for the $O(^3P) + H_2 \rightarrow OH + H$ reaction using the approximate quantum potential. The latter is defined by the nonclassical component of the momentum operator expanded in terms of linear and exponential functions. Unlike earlier implementations with linear functions, the introduction of the exponential function provides an accurate description of asymptotic dynamics for this system and gives good agreement of approximate reaction probabilities with accurate quantum calculations.

1. Introduction

The standard methods of quantum molecular dynamics based on a grid or basis representation of the wave function are not feasible for systems beyond 10−12 degrees of freedom due to exponential scaling of the numerical effort with system size. At the same time, classical molecular dynamics is widely used to study systems of hundreds of atoms, but it is incapable of capturing quantum-mechanical (QM) effects, such as nonadiabatic dynamics and the quantum behavior of hydrogen atoms. Therefore, the development of rigorous semiclassical methods that combine favorable scaling of classical mechanics with respect to system size with an accurate QM description of molecular motion is a long-standing goal of theoretical chemistry.

In semiclassical methods, the nonlocality of quantum mechanics can be introduced through local high-order expansions, such as the second-order expansion of the potential in the Initial Value Representation methods.[1,2] Alternatively, the influence of nonlocality on the dynamics can be included via ensemble or density averaged effective potentials as in the Ehrenfest-type methods.[3] Phase space formulations with initial conditions satisfying the uncertainty principle can also describe some quantum effects. For example, the Wigner method[4,5] gives the correct QM evolution of the harmonic oscillator, even though propagation of trajectories is purely classical. From practical considerations, it is desirable to have a semiclassical method that has a well-defined classical limit, is improvable toward the exact QM limit, has favorable scaling with system size, and does not require evaluation of Hessians. This means that a trajectory description and a coordinate space representation of a wave function are essential for such a method.

The hydrodynamic or de Broglie−Bohm formulation[6] of the time-dependent Schrödinger Equation (SE), which provides this framework, has gained a considerable attention in recent years as an alternative approach to quantum dynamics. The formulation, which is formally equivalent to the standard SE, is based on the polar form of the wave function

$$\psi = A(x, t) \exp(\triangle S(x, t)/\hbar)$$

and leads to the representation of ψ in terms of quantum trajectories propagated according to the laws of classical mechanics. All QM effects are incorporated through the quantum potential:

$$U = -\frac{\hbar^2}{2m}\frac{\nabla^2 A(x, t)}{A(x, t)}$$

which is added to the classical potential in the equations of motion (m is a mass of a particle). Exact implementation of this formalism is generally impractical due to the complicated and, possibly, singular quantum potential, but the quantum trajectory framework is conceptually appealing: the trajectories can be interpreted as the optimal set of grid points tracking the dynamics of the wave function density. Following multidimensional implementation of the de Broglie−Bohm formulation using stationary grids by Dey et al.[7] and the introduction of the quantum trajectory method by Lopreore and Wyatt,[8] a variety of exact and approximate approaches have been suggested in coordinate space[9−14] and in phase space.[15−21]

For nodeless wave function densities, the quantum potential vanishes in the classical limit of large mass. Therefore, the quantum trajectory framework provides a natural connection to classical mechanics and a convenient starting point for semiclassical approximate approaches. Recently, Garashchuk and Rassolov pursued the idea of using a globally determined approximate quantum potential (AQP).[22−25] The semiclassical framework allows one to include the leading quantum effects on dynamics by averaging over the wave function density, including possible singularities in the exact quantum potential, and ensures stable dynamics. The method has a well-defined classical limit of zero AQP and the QM limit of a highly accurate AQP. In its simplest (quadratic) form, the AQP is exact for Gaussian wave packets in locally quadratic potentials, which is a typical representation of moving nuclei. In more general

† Part of the special issue "John C. Light Festschrift".

* Corresponding author. E-mail: sgarashc@mail.chem.sc.edu.
‡ University of South Carolina.
§ Northwestern University.

10.1021/jp056741+ CCC: $33.50
Published on Web 03/08/2006

systems it describes tunneling, zero-point energy, and isotope effects as was shown for two-dimensional models of ICN and H_3. The accuracy of the approximate description can be improved by using better than quadratic globally defined AQPs or by defining quadratic AQPs on subspaces.[26] In the latter case, the nonclassical momentum can be linearized on several subspaces or domains using weighting functions $h_i(x)A^2(x, t)$ in which moments of the trajectory distribution determine the AQP parameters. The non-negative domain functions $h_i(x)$ describing, for example, the reaction channels and interaction region of a potential electronic surface or the anharmonic regions of a potential, are chosen to add up to one, $\sum_i h_i(x) = 1$. Interference and nonadiabatic dynamics which are intrinsically quantum effects can be efficiently described using a mixed polar/coordinate space wave function representation:[27−29] the overall wave function is represented in terms of density and phase associated with the quantum trajectory dynamics, while nonadiabatic wave function transfer and the wave function nodes are described through a coordinate space prefactor.

In the formalism of ref 25, the quadratic AQP is defined using a linear approximation $\tilde{r}$ to the nonclassical momentum r:

$$r = \nabla A(x, t)/A(x, t)$$

Parameters of $\tilde{r}$ are found variationally from the moments of the trajectory distribution by means of linear algebra for any number of dimensions or subspaces. The total energy in closed systems is conserved. The quantum force for all trajectories is obtained analytically from the AQP once every time step. The number of moments scales quadratically with the system size if correlation between all degrees of freedom is considered, but the overall numerical cost of propagation is dominated by the propagation of trajectories, which has a weaker dependence than quadratic. The initial wave function density can be sampled according to the standard methods of multidimensional integration including Monte Carlo techniques. These features make the AQP method well-suited for high-dimensional problems that can be formulated in terms of localized initial wave functions and defined in Cartesian or Cartesian-like coordinates. However, it is often useful to have simple asymptotic motion such as uncoupled rovibrational motion of reaction fragments achieved in non-Cartesian coordinates. A proper treatment of symmetry can also be very important. Our preliminary studies of atom + diatom collisions in Cartesian coordinates (with the center-of-mass motion subtracted) using Gaussian initial wave packets for collinear configurations have shown large differences between classical and AQP results even at large incident energies. We attribute this effect to the fact that while in the classical treatment, $U = 0$, the trajectories remain coplanar, in the AQP treatment, the quantum trajectories spread in full six-dimensional space. Use of coordinate systems with non-orthogonal kinetic energy,[30] for instance, the bond coordinate system in spectroscopy, has also served as a motivation to generalize the quantum trajectory formulation to arbitrary coordinate systems, as presented in Section 2.

We test the AQP approach in curvilinear coordinates by computing the wave packet reaction probabilities for $O(^3P) + H_2$ ($v = 0, j = 0$) $\rightarrow$ OH + H reaction in three dimensions for zero total angular momentum on the $^3A'$ and $^3A''$ surfaces of Rogers et al.[31] The quantum trajectory formulation and the definition of a simple AQP in angular coordinates are given in Section 3. An improved AQP description for vibrational degrees of freedom is described in Section 4. Results for the O + H_2 and O + HD dynamics are presented in Section 5. Section 6 concludes the paper.

2. Quantum Trajectories in Arbitrary Coordinates

For a general curvilinear system of coordinates $\{\vec{x}\}$, the kinetic energy operator $\hat{T}$ is

$$\hat{T} = \frac{1}{2}\nabla^{\dagger}\mathbf{G}\nabla \tag{1}$$

Here ∇ is the gradient operator of a general form:

$$\nabla_i = f_i(\vec{x})\frac{\partial}{\partial x_i} \tag{2}$$

and $\nabla^{\dagger}$ acts on the left. **G** is an inverse matrix of masses and moments of inertia. In general, **G** can have off-diagonal elements. In chemical applications, a system of coordinates is often chosen to eliminate derivative cross-terms in the Hamiltonian, so that asymptotic motion of fragments is uncoupled. This means that the matrix **G** is diagonal. Typical coordinates for these applications are the Jacobi or Radau coordinates in spectroscopy or reactive scattering calculations.[32] The derivation below is given for the diagonal form of **G**, but it can be extended to the nondiagonal case in a straightforward manner. We use atomic units, $\hbar = 1$, throughout, and the $\hbar$ dependence is noted where it is important for interpretation. For square-integrable wave functions, taking into account the Jacobian $J = J(\vec{x})$ of the transformation from Cartesian coordinates to a given set of coordinates, eq 1 can be rewritten as

$$\hat{T} = -\frac{1}{2}(\nabla^T\mathbf{G}\nabla + \vec{d}^T\mathbf{G}\nabla) \tag{3}$$

The components of the vector $\vec{d}$ are

$$d_i = \frac{\partial f_i}{\partial x_i} + \frac{f_i}{J}\frac{\partial J}{\partial x_i} \tag{4}$$

The hydrodynamic or Bohmian form of the SE is based on the representation of a wave function in terms of real phase and amplitude or density:

$$\psi(\vec{x}, t) = A(\vec{x}, t)\exp(\iota S(\vec{x}, t)) = \sqrt{\rho(\vec{x}, t)}\exp(\iota S(\vec{x}, t)) \tag{5}$$

Substitution of eq 5 into the SE and separation into real and imaginary parts gives the following equations:

$$\frac{\partial S}{\partial t} + \frac{1}{2}(\nabla S)^T\mathbf{G}(\nabla S) + V + U = 0 \tag{6}$$

$$U = -\frac{1}{2A}(\nabla^T\mathbf{G}(\nabla A) + \vec{d}^T\mathbf{G}(\nabla A)) \tag{7}$$

and

$$\frac{\partial \rho}{\partial t} + (\nabla S)^T\mathbf{G}(\nabla \rho) + \nabla^T\mathbf{G}\nabla S\rho + \vec{d}^T\mathbf{G}(\nabla S)\rho = 0 \tag{8}$$

U is the quantum potential which is, formally, the only $\hbar^2$ term becoming small in the classical limit $\hbar \rightarrow 0$. All other terms do not depend explicitly upon $\hbar$. We can define a full time derivative as

$$\frac{d}{dt} = \frac{\partial}{\partial t} + (\nabla S)^T\mathbf{G}(\nabla) = \frac{\partial}{\partial t} + \sum_i v_i\frac{\partial}{\partial x_i} \tag{9}$$

in the frame of reference moving with the velocity

$$v_i = \frac{\partial S}{\partial x_i} G_{ii} f_i^2 \tag{10}$$

Then, eq 8 becomes

$$\frac{\mathrm{d}\rho}{\mathrm{d}t} = -(\nabla^T \mathbf{G}(\nabla S) + \vec{d}^T \mathbf{G} \nabla)\rho \tag{11}$$

Differentiating eq 6 with respect to x_i and using eq 9 one obtains

$$\frac{d}{\mathrm{d}t}\frac{\partial S}{\partial x_i} + \sum_k G_{kk} f_k \frac{\partial f_k}{\partial x_i}\left(\frac{\partial S}{\partial x_k}\right)^2 + \frac{\partial}{\partial x_i}(V+U) = 0 \tag{12}$$

If derivatives of the phase are identified with the momentum

$$p_i = \frac{\partial S}{\partial x_i} \tag{13}$$

and the phase S is identified with the classical action function, then for any form of the gradient operator eqs 6, 10, and 12 give time dependence of $\vec{x}$, $\vec{p}$, and S:

$$\frac{\mathrm{d}x_i}{\mathrm{d}t} = G_{ii} f_i^2 p_i \tag{14}$$

$$\frac{\mathrm{d}p_i}{\mathrm{d}t} = -\frac{\partial}{\partial x_i}(V+U) - \sum_k G_{kk} f_k \frac{\partial f_k}{\partial x_i} p_k{}^2 \tag{15}$$

$$\frac{\mathrm{d}S}{\mathrm{d}t} = \frac{1}{2}\sum_k G_{kk} f_k{}^2 p_k{}^2 - (V+U) \tag{16}$$

Equations 14−16 are consistent with classical equations of motion of a trajectory governed by the Hamiltonian:

$$H = \frac{1}{2}\sum_k G_{kk} f_k{}^2 p_k{}^2 + V + U \tag{17}$$

For a nondiagonal form of the matrix **G**, the equations of motion correspond to the Hamiltonian of eq 17 with the single summation replaced by the double sum, $\sum_{kl} G_{kl} f_k f_l p_k p_l$.

Importantly, the density of a wave function "carried" by a trajectory within the associated volume element $J\Omega$, $\Omega = \Pi_i \delta x_i$, or the trajectory weight

$$w = \rho J \Omega \tag{18}$$

is conserved in closed systems as has been the case in Cartesian coordinates:[23]

$$\frac{\mathrm{d}w}{\mathrm{d}t} = \frac{\mathrm{d}\rho}{\mathrm{d}t} J\Omega + \rho \frac{\mathrm{d}J}{\mathrm{d}t}\Omega + \rho J \frac{\mathrm{d}\Omega}{\mathrm{d}t} = 0 \tag{19}$$

This can be verified by using eqs 9−11 to define time derivatives in eq 19:

$$\frac{\mathrm{d}J}{\mathrm{d}t} = (\nabla S)^T \mathbf{G} (\nabla J) \tag{20}$$

$$\frac{\mathrm{d}\Omega}{\mathrm{d}t} = \sum_k \frac{\delta v_k}{\delta x_k}\Omega = \left(\nabla^T \mathbf{G}(\nabla S) + \sum_k \frac{\partial f_k}{\partial x_k} G_{kk} f_k p_k\right)\Omega \tag{21}$$

The weight conservation property means that one does not need to solve eq 11 involving gradients of $\vec{p}$ and ρ to determine the time dependence of the density. Moreover, the expectation value of an operator that is local in the coordinate representation, such as the wave packet probability, can be found by simple summation over the trajectory weights, $\langle \hat{O} \rangle = \sum_n O(\vec{x}_n) w_n$.

Equations 14−16 and 19 give a local description of quantum dynamics with the exception of the nonlocal quantum potential U given by eq 7. This is the quantity that vanishes in the classical limit of small $\hbar$ and large mass for nodeless wave function densities. We determine U approximately in order to make the quantum trajectory framework practical in large systems, while retaining the dominant quantum effects. It is convenient to define U in terms of the nonclassical component of the gradient operator:

$$\vec{r} = \frac{\nabla A(x,t)}{A(x,t)}. \tag{22}$$

Then, the quantum potential in an arbitrary system of coordinates becomes

$$U = -\frac{1}{2}(\vec{r}^T \mathbf{G} \vec{r} + \nabla^T \mathbf{G} \vec{r} + \vec{d}^T \mathbf{G} \vec{r}) \tag{23}$$

The nonclassical momentum $\vec{r}$ is the only quantity that will be approximated in the course of dynamics.

3. Trajectory Formulation for Three-Dimensional Jacobi Coordinates

A. Equations of Motion. Let us apply the formalism of Section 2 to a nonrotating triatomic molecule described in the Jacobi coordinates $\{x, y, \theta\}$ where y is the diatomic internuclear separation, x is the distance between the third atom and the center of mass of the diatomic, and θ is the angle between x and y. The motion of the center of mass is subtracted, and the total angular momentum is set to zero. The SE is typically solved for the wave function scaled by xy so that the volume element is

$$J\Omega = \sin\theta \delta\theta \, \delta x \, \delta y \tag{24}$$

The QM Hamiltonian is

$$\hat{H} = -\frac{1}{2M}\frac{\partial^2}{\partial x^2} - \frac{1}{2m}\frac{\partial^2}{\partial y^2} - \frac{1}{2\mu}\left(\frac{\partial^2}{\partial \theta^2} + \cot\theta \frac{\partial}{\partial \theta}\right) + V \tag{25}$$

with the moments of inertia included as

$$\frac{1}{\mu} = \frac{1}{Mx^2} + \frac{1}{my^2} \tag{26}$$

For the given $\hat{H}$, the derivative operators (2) and (4) are

$$\nabla^T = \left(\frac{\partial}{\partial x}, \frac{\partial}{\partial y}, \frac{\partial}{\partial \theta}\right), \quad \vec{d}^T = (0, 0, \cot\theta) \tag{27}$$

The matrix **G** has three nonzero components on the diagonal $\{M^{-1}, m^{-1}, \mu^{-1}\}$. Substitution of the polar form of the wave function

$$\psi(x, y, \theta, t) = A(x, y, \theta, t) \exp(\iota S(x, y, \theta, t)) \tag{28}$$

into the SE and identification $\nabla S = \vec{p}$, lead to the following expressions for the time evolution of the phase and density:

$$\frac{dS}{\partial t} = \frac{p_x^2}{2M} + \frac{p_y^2}{2m} + \frac{p_\theta^2}{2\mu} - V - U \tag{29}$$

$$\frac{d\rho}{dt} = -\left(\frac{1}{M}\frac{\partial p_x}{\partial x} + \frac{1}{m}\frac{\partial p_y}{\partial y} + \frac{1}{\mu}\frac{\partial p_\theta}{\partial \theta} + \frac{\cot\theta}{\mu}p_\theta\right)\rho \tag{30}$$

The full time-derivative is defined as in eq 9:

$$\frac{d}{dt} = \frac{\partial}{\partial t} + \frac{p_x}{M}\frac{\partial}{\partial x} + \frac{p_y}{m}\frac{\partial}{\partial y} + \frac{p_\theta}{\mu}\frac{\partial}{\partial \theta} \tag{31}$$

U is the quantum potential defined by eq 23 in terms of the nonclassical momentum $\vec{r} = A^{-1}\nabla A$. The trajectory weights w defined by eqs 18 and 24 are constant in time for closed systems as shown in Section 2 and can be used instead of solving eq 30.

B. Angle-Dependent AQP. The linearized nonclassical momentum gives a useful and cheap global approximation to the quantum potential for the dynamics in Cartesian coordinates.[25] In this approach the nonclassical momentum $\vec{r}$ is represented by a linear function of the coordinates, whose parameters are found from the linear matrix equation in terms of the first and second moments of the trajectory distribution. The procedure is variational and, thus, conserves total energy for a closed system. The corresponding AQP is exact for the correlated Gaussian wave packets that are often used to represent the ground vibrational state and localized wave function in the translational degree of freedom. In principle, a linear combination of Gaussian wave packets can also represent other localized wave functions.[33] It was also shown that the accuracy of this approach can be improved by defining a linearized nonclassical momentum on subspaces[26] and that the use of mixed coordinate/polar representation of the wave function enables one to describe nonadiabatic dynamics[27,28] as well as to describe density nodes[29] in an efficient manner.

For a description in Jacobi coordinates, we extend the idea of the linearized nonclassical momentum to include the angle. In Cartesian coordinates, the use of the linear approximation to the nonclassical momentum was motivated by the fact that this treatment is exact in the important limiting case of an eigenstate of the harmonic oscillator. Description of r_θ as a linear function of θ can still be appropriate in some cases, such as applications in spectroscopy, if the initial state is chosen as a localized Gaussian function of the bending angle.[34]

In reactive scattering, the initial condition associated with rotation of the diatomic molecule is typically a rotational eigenstate. The lowest state, $j = 0$, has zero nonclassical momentum so using $\tilde{r}_\theta = 0$ in AQP already describes a physically relevant approximation. To introduce the dependence on the angle while keeping computation of AQP numerically efficient and avoiding singular terms, we choose the parameters of the linearized r_x and r_y to be linear functions of $\cos\theta$. This functional form of approximate $\tilde{r}$ corresponds to a functional form of a wave function amplitude:

$$\tilde{A} = C\exp(-\vec{R}^T\mathbf{B}\vec{R} - \cos\theta\vec{R}^T\mathbf{B}'\vec{R}) \tag{32}$$

where $\vec{R}^T = (x - x_0, y - y_0)$ and $\mathbf{B}$ and $\mathbf{B}'$ are symmetric matrixes. C is a normalization factor; x_0, y_0, and the matrix elements are parameters. (The amplitude $\tilde{A}$ is never used in dynamics.) Then, using $\tilde{r} = \tilde{A}^{-1}\nabla\tilde{A}$, the basis for expansion of r_x and r_y is

$$\vec{\eta}_R{}^T = \{1, x, y, \cos\theta, x\cos\theta, y\cos\theta\} \tag{33}$$

while the basis for r_θ is

$$\vec{\eta}^T{}_\theta = \{1, x, y, xy, x^2, y^2\} \tag{34}$$

Approximations to the radial components are $\tilde{r}_x = \vec{c}_x{}^T\vec{\eta}_R$ and $\tilde{r}_y = \vec{c}_y{}^T\vec{\eta}_R$. Optimization of the coefficients $\vec{c}_x$ and $\vec{c}_y$ is completely analogous to the procedure in Cartesian coordinates.[26] The approximation to the angular component is $\tilde{r}_\theta = \sin\theta\vec{c}^T{}_\theta\vec{\eta}_\theta$. Optimal parameters $\vec{c}_\theta$ are found from minimization of the error functional, $f_\Omega(r_\theta - \tilde{r}_\theta)^2a^2\delta\Omega$, whose parameter-dependent part after integration by parts becomes

$$I = \int_\Omega\left(\frac{\partial\tilde{r}_\theta}{\partial\theta} + \tilde{r}_\theta\cot\theta + \tilde{r}_\theta^2\right)a^2\delta\Omega \tag{35}$$

Ω is the volume of integration and the volume element is $\delta\Omega = \sin\theta\, d\theta\, dx\, dy$. For the basis given by eq 34, all integrals in eq 35 are nonsingular and can be expressed as sums over the trajectory weights:

$$I \approx \sum_n(2\vec{c}_\theta{}^T\vec{\eta}_\theta\cos\theta_n + \vec{c}_\theta{}^T\vec{\eta}_\theta\vec{\eta}_\theta{}^T\vec{c}_\theta\sin^2\theta_n)w_n \tag{36}$$

Minimization of eq 36 with respect to $\vec{c}_\theta$ gives the optimal parameter values

$$\vec{c}_\theta = -\langle\vec{\eta}_\theta\vec{\eta}_\theta{}^T\sin^2\theta\rangle^{-1}\langle\vec{\eta}_\theta\cos\theta\rangle \tag{37}$$

Note that eq 35 is proportional to the contribution of r_θ to the quantum potential; therefore, its minimization results in conservation of total energy.[24]

4. Accurate Description of Asymptotic Motion

The time evolution of wave functions for bound potentials presents a major challenge for quantum trajectory methods,[35,14] with the exception of Gaussian wave packets evolving in harmonic potentials. Since zero-point energy is often a leading quantum effect in large molecular systems, efficient description of wave packet dynamics in anharmonic potentials is highly desirable. In anharmonic systems, the accuracy of the quantum potential quickly (depending on anharmonicity) deteriorates with time and trajectories decohere even for the ground-state initial wave function. In theory, the positions of the quantum trajectories representing an eigenstate remain unchanged, because the quantum potential compensates the classical potential V up to an additive constant. Numerically, such perfect compensation is difficult to achieve, which leads to the rapid error accumulation as trajectories begin to move. One way addressing this problem—a truncated Taylor expansion of the potential allowing for exact cancellation of the classical and quantum forces—was suggested in ref 14. In the context of AQP, linearization of the nonclassical momentum on subspaces increases the accuracy of the quantum potential and extends the duration of accurate dynamics, though a large number of subspaces are required for perfect cancellation of the classical and quantum forces.[26]

In reactive scattering, we can also improve description of the asymptotic vibrational states by explicitly including a suitable basis function in the expansion of the nonclassical momentum. Diatomic molecules are often represented as particles of reduced mass m governed by a Morse potential[36]:

$$V = D(1 - \zeta)^2 \quad \zeta = \exp(-z(x - x_m)) \tag{38}$$

The nonclassical momentum for the lowest eigenstate of the Morse oscillator is

$$r = \sqrt{2Dm}(\zeta - 1) + \frac{z}{2} \tag{39}$$

and the same as eq 39 different only in the constant for higher eigenstates. Note that for an integrable wave function the slope of r in eq 39 is positive. It is especially important that r is a linear function with respect to ζ. Therefore, including the function ζ into the expansion basis of r, $\tilde{r} = \vec{c}^T\vec{\eta}$, $\vec{\eta} = \{1, x, \zeta\}$, gives the exact quantum potential for the eigenstates of the Morse oscillator and should increase accuracy for other anharmonic potentials that are reasonably approximated by a Morse potential in the region of nonzero wave function density. Optimization of the expansion coefficients $\vec{c}$ is the same as described in ref 25 for the linear basis set.

As a numerical example, we compute the autocorrelation function of the ground state of the nonrotating H_2 molecule. The corresponding potential exhibits a large degree of anharmonicity even at low energies. The potential is defined by eq 38 with parameter values taken from LSTH surface:[37,38] $m = 925.26\ m_e$, $D = 0.1663$ hartree, $z = 1.1\ a_0^{-1}$, and $x_m = 1.41\ a_0$. Figure 1a shows the real part of the autocorrelation function computed from trajectories using

$$C(2t) = \sum_i w_i \exp(2\imath S_i(t)) \tag{40}$$

for six oscillations. The initial wave function is

$$\psi(x, 0) = (2\lambda\zeta k)^{\lambda - 1/2} \exp(-\lambda\zeta) \quad \lambda = \sqrt{2Dm}/z \tag{41}$$

where $k = 0.009087$ is the normalization factor. Figure 1b shows the corresponding quantum trajectories that are completely stable. Figure 1, panels c and d, shows propagation of the Gaussian wave packet, which is the ground state of the harmonic approximation to this Morse potential:

$$\psi(x, 0) = \left(\frac{2\alpha}{\pi}\right)^{1/4} \exp(-\alpha(x - x_m)^2) \tag{42}$$

with the parameter $\alpha = 9.66\ a_0^{-2}$. The agreement of the autocorrelation function, which is similar to that of the Morse eigenstate, is very good. This is a dramatic improvement over the AQP computation with the basis of linear functions, where trajectories and, consequently, $C(t)$ decohere after half of the oscillation period due to the strong anharmonicity. Figure 1d shows the error accumulation as a function of time in the absolute value of $C(t)$ for the bases with and without ζ.

Use of the exponential function for the description of vibrational dynamics will make the propagation more accurate in many cases, because the lowest eigenstate serves as a basis for coherent states of the Morse potential[39] and because the nonclassical momentum of the excited states is a linear function of ζ. The basis function $\zeta = \exp(-z(x - x_m))$ has just one parameter since the shift by x_m is equivalent to multiplication of ζ by a constant optimized in the expansion procedure. The parameter z can be chosen from the approximation, possibly a time-dependent one, to the classical potential in the regions of nonzero density. Optimization of z along with the expansion coefficients $\vec{c}$ is also a possibility. This, however, is a nonlinear optimization and may add significant cost to an otherwise efficient method.

5. Dynamics of $O(^3P) + H_2$ in Three Dimensions

As a test of the non-Cartesian quantum trajectory approach, we compute wave packet reaction probabilities for the $O(^3P) + H_2(v = 0, j = 0) \rightarrow OH + H$ system on the $^3A'$ and $^3A''$ potential energy surfaces of Rogers et al.[31] This system has been extensively studied in recent years, in both theoretical and experimental work.[40−44] In this study, we are interested in the low-energy regime where tunneling plays an important role. The wave packet reaction probabilities are computed as the sum over trajectories in the product region:

$$P = \sum_i w_i(R_i < R_0)$$

where $R_0 = 3.5\ a_0$ and R_i is the bond length of OH as a function of time. The propagation is terminated once P stops changing in time. The initial wave packet is a direct product of the Gaussian in the translational coordinate and the ground state in the internal degrees of freedom:

$$\psi(x, y, \theta, 0) = \left(\frac{\alpha}{\pi}\right)^{1/4} \exp(-\alpha(x - x_0)^2 + \imath p_0(x - x_0))\chi(y) \tag{43}$$

The translational parameters are $\alpha = 4\ a_0^{-2}$, $x_0 = 6\ a_0$, $p_0 = [6, 20]$. $\chi(y)$ is the ground vibrational state represented as a Gaussian:

$$\chi(y) = \left(\frac{\beta}{\pi}\right)^{1/4} \exp(-\beta(y - y_0)^2) \tag{44}$$

with numerical parameters $y_0 = 1.44\ a_0$ and $\beta = 9.06\ a_0^{-2}$. The calculations were performed using 5000 trajectories with pseudo-random sampling in three dimensions.[45] We find that the θ-component of $\vec{r}$ is small as compared to the radial components and can be neglected. The classical probabilities are obtained by setting the quantum potential to zero. A comparison is made with time-dependent quantum calculations that we have performed using the split-operator method[46,47] with a grid representation for x and y and the Discrete Variable Representation[48] for θ. The grid is 256×256 points with a spacing of $0.08\ a_0$. The number of the DVR points is between 45 and 80 depending on the energy of the wave packet. The AQP calculations are about 9 times faster than the quantum propagation with 45 DVR points.

Exact QM and trajectory probabilities for the two surfaces are presented in Figure 2 for one of the equivalent reaction channels. The discrepancy between the quantum and classical results is the most pronounced at lower energies. The errors in classical probabilities for energies below 0.8 eV are about twice as large for the $^3A''$ surface than for $^3A'$. A quadratic AQP obtained from linearization of the nonclassical momentum $\vec{r}$ described in Section 3.B corrects probabilities at energies below 0.3 eV but underestimates probabilities at higher energies. The agreement between the trajectory and quantum results is significantly improved when the exponential function, $\zeta = \exp(-zy)$, is introduced into the radial basis as described in Section 4. The parameter z was set to a value of the vibrational potential in the reactant channel, $z = 1.1\ a_0^{-1}$. Evidently, the additional basis function improves the description of the asymptotic dynamics and also contributes to the description at the transition state. The expansion coefficient of ζ was constrained to be nonnegative, so that the resulting $\tilde{r}$ would be consistent with a normalizable wave function, eq 39. The accuracy of the AQP calculations on the two potential energy surfaces is comparable.

Figure 3 shows probabilities for the isotopically substituted reaction $O + HD \rightarrow OH(D) + D(H)$ as a function of the translational energy. Here the width parameter of the initial vibrational state of HD is taken to be $\beta = 10.46\ a_0^{-2}$. The probability for producing the OD + H fragments is relatively

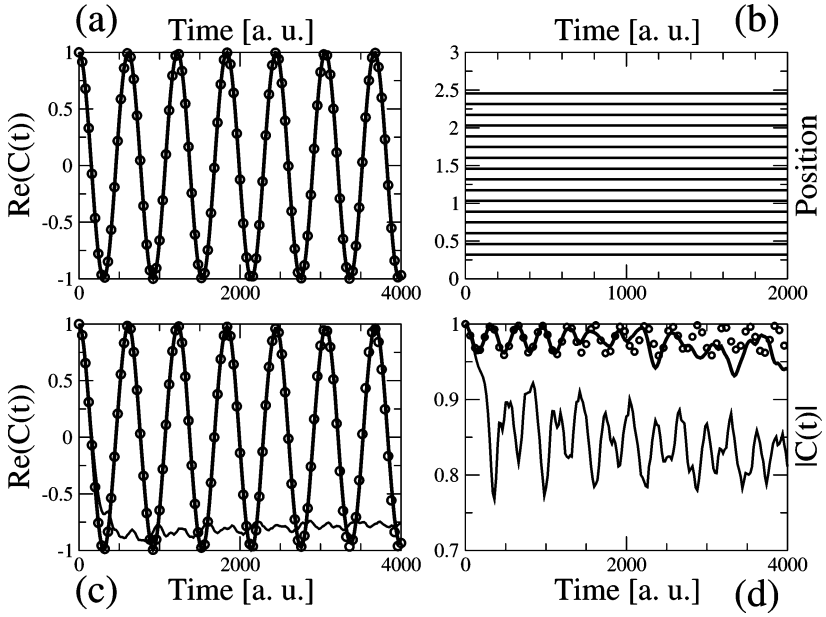

Figure 1. Autocorrelation function, $C(t) = \langle\psi(0)|\psi(t)\rangle$, of a wave packet in the Morse potential. (a) $\mathscr{R}(C(t))$ of the ground eigenstate using QM (circles) and AQP with exponential basis function (line) propagations. (b) Quantum trajectories for the ground eigenstate obtained with the AQP method. (c) $\mathscr{R}(C(t))$ of the Gaussian wave packet using QM (circles), AQP with (thick line) and without (thin line) exponential basis function. (d) $|C(t)|$ of the Gaussian wave packet. Legend is the same as in panel c.

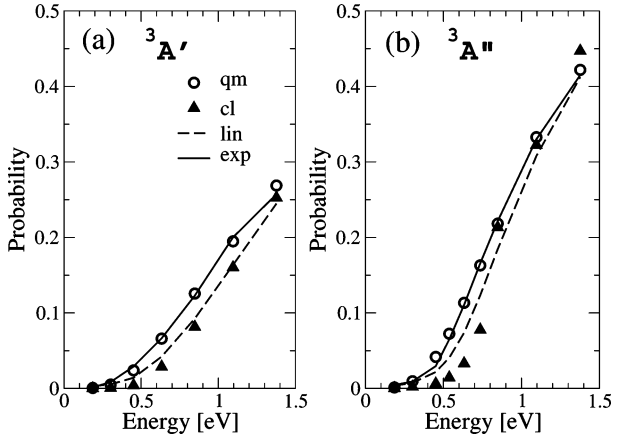

Figure 2. Wave packet reaction probabilities for the O + H $_2$($v = 0$, $j = 0$) → OH + H reaction on (a) $^3A'$ and on (b) $^3A''$ potential surfaces as a function of the translational energy. Results for QM (circles), classical (triangles), AQP with linear basis (dash), and AQP with the added exponential function (solid line) methods are shown on both panels.

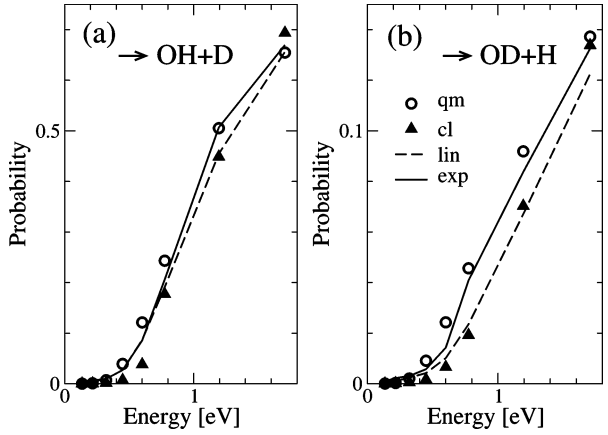

Figure 3. Wave packet reaction probabilities for (a) O + HD ($v = 0$, $j = 0$) → OH + D and (b) O + HD ($v = 0$, $j = 0$) → OD + H reaction on $^3A'$ surface. Results for QM (circles), classical (triangles), AQP with linear basis (dash), and AQP with the added exponential function (solid line) methods are shown on both panels. Note the difference in scale of the vertical axis.

low (about 20% of that for OH + D), so 15000−20000 trajectories per wave packet have been propagated to generate the results. The quadratic AQP calculation gives a larger correction to the probabilities of the OH channel as compared to that of the OD channel, most likely because the discrepancy between the quantum and classical results is larger for OH. Use of the exponential function in y gives good agreement between the quantum and trajectory results for both channels.

6. Conclusions

We have generalized the quantum trajectories approach to propagation of the wave function in an arbitrary coordinate system. This allows us to take advantage of the uncoupling of partial waves in reactive scattering problems, to use nonorthogonal coordinate systems, such as bond coordinates in theoretical spectroscopy, and to use initial conditions with well-defined vibrational and rotational quantum numbers, as appropriate for simulating many experiments. This approach has been implemented using the approximate quantum potential (AQP) method, which was extended to applications in distance-angle variables. We have also improved the AQP description of asymptotic motion of vibrational eigenstates by including the exponential function into the approximation procedure. This new feature allows for an exact treatment of the Morse oscillator eigenstates. Its application to other types of bound potentials and initial wave functions will be explored in future work.

The AQP method was implemented in three-dimensional Jacobi coordinates to treat a nonrotating O + H_2 system. We have computed the wave packet reaction probabilities for the O(^{3}P) + H_2 → OH + H reaction for the ground state of the reagents. Overall, the classical calculation (performed by setting AQP to zero) gives probabilities that are well below the exact quantum results at energies close to threshold, though they approach QM results at high energies. Quadratic AQP obtained with the linear basis corrects the low energy regime in a manner

consistent with an earlier application to the collinear hydrogen exchange reaction.[25] This form of AQP gives a larger correction on the $^3A''$ surface, which is consistent with the more significant tunneling associated with this surface. Addition of the exponential function to the expansion basis for the nonclassical momentum determining the AQP, further improves the semiclassical probabilities, resulting in very good agreement with the QM probabilities on both surfaces. The trajectory probabilities are obtained using 5000 trajectories. We observe similar accuracy of the AQP results for the O + HD reaction, although due to low probabilities in the OD + H channel three times as many trajectories are required for convergence. For a typical trajectory propagation, 1−2% of computer time is spent on the AQP computation. The accuracy and scaling properties of the AQP method will be further explored in studies of nonadiabatic dynamics for this reaction and in applications to larger molecular systems.

Acknowledgment. We acknowledge the Chemistry Division of NSF and AFOSR MURI for support of this research and thank R. E. Wyatt for useful comments on the manuscript.

References and Notes

(1) Herman, M.; Kluk, E. *Chem. Phys.* **1984**, *91*, 27.
(2) Kay, K. G. *J. Chem. Phys.* **1994**, *100*, 4377−4392.
(3) Tully, J. C. *Faraday Discuss.* **1998**, *110*, 407−419.
(4) Wigner, E. P. *Phys. Rev.* **1932**, *40*, 749.
(5) Heller, E. J. *J. Chem. Phys.* **1976**, *65*, 1289−1298.
(6) Bohm, D. *Phys. Rev.* **1952**, *85*, 166−193.
(7) Dey, B. K.; Askar, A.; Rabitz, H. *J. Chem. Phys.* **1998**, *109*, 8770−8782.
(8) Lopreore, C. L.; Wyatt, R. E. *Phys. Rev. Lett.* **1999**, *82*, 5190−5193.
(9) Bittner, E. R. *J. Chem. Phys.* **2000**, *112*, 9703−9710.
(10) Wyatt, R. E.; Bittner, E. R. *J. Chem. Phys.* **2000**, *113*, 8898−8907.
(11) Kendrick, B. K. *J. Chem. Phys.* **2003**, *119*, 5805−5817.
(12) Babyuk, D.; Wyatt, R. E. *J. Chem. Phys.* **2004**, *121*, 9230−9238.
(13) Poirier, B. *J. Chem. Phys.* **2004**, *121*, 4501−4515.
(14) Liu, J.; Makri, N. *J. Phys. Chem. A* **2004**, *108*, 5408−5416.
(15) Burghardt, I.; Cederbaum, L. S. *J. Chem. Phys.* **2001**, *115*, 10303−10311.
(16) Burghardt, I.; Cederbaum, L. S. *J. Chem. Phys.* **2001**, *115*, 10312−10322.
(17) Burghardt, I.; Moller, K. B. *J. Chem. Phys.* **2002**, *117*, 7409−7425.
(18) Maddox, J. B.; Bittner, E. R. *J. Phys. Chem. B* **2002**, *106*, 7981−7990.
(19) Bittner, E. R.; Maddox, J. B.; Burghardt, I. *Int. J. Quantum Chem.* **2002**, *89*, 313−321.
(20) Donoso, A.; Martens, C. C. *Phys. Rev. Lett.* **2001**, *87*, 223202.
(21) Trahan, C. J.; Wyatt, R. E. *J. Chem. Phys.* **2003**, *119*, 7017−7029.
(22) Garashchuk, S.; Rassolov, V. A. *Chem. Phys. Lett.* **2002**, *364*, 562−567.
(23) Garashchuk, S.; Rassolov, V. A. *J. Chem. Phys.* **2003**, *118*, 2482−2490.
(24) Garashchuk, S.; Rassolov, V. A. *Chem. Phys. Lett.* **2003**, *376* (3−4), 358−363.
(25) Garashchuk, S.; Rassolov, V. A. *J. Chem. Phys.* **2004**, *120*(3), 1181−1190.
(26) Rassolov, V. A.; Garashchuk, S. *J. Chem. Phys.* **2004**, *120*(15), 6815−6825.
(27) Rassolov, V. A.; Garashchuk, S. *Phys. Rev. A* **2005**, *71* (3), 032511.
(28) Garashchuk, S.; Rassolov, V. A.; Schatz, G. C. *J. Chem. Phys.* **2005**, *123*, 174108.
(29) Garashchuk, S.; Rassolov, V. A. *J. Chem. Phys.* **2004**, *121* (18), 8711−8715.
(30) Mladenovic, M. *J. Chem. Phys.* **2000**, *112*, 1082−1094.
(31) Rogers, S.; Wang, D.; Kuppermann, A.; Walch, S. *J. Phys. Chem. A* **2000**, *104*, 2308−2325.
(32) Mladenovic, M. *J. Chem. Phys.* **2000**, *112*, 1070−1081.
(33) Henriksen, N. E.; Heller, E. J. *J. Chem. Phys.* **1989**, *91*, 4700−4713.
(34) Sun, X.; Miller, W. H. *J. Chem. Phys.* **1998**, *108*, 8870−8877.
(35) Bittner, E. R. *J. Chem. Phys.* **2003**, *119*, 1358−1364.
(36) Morse, P. M. *Phys. Rev.* **1929**, *34*, 57−65.
(37) Siegban, P.; Liu, B. *J. Chem. Phys.* **1978**, *68*, 2457.
(38) Truhlar, D. G.; Horowitz, C. J. *J. Chem. Phys.* **1978**, *68*, 2466.
(39) Cooper, I. L. *J. Phys. A* **1991**, *25*, 1671−1683.
(40) Robie, D. C.; Arepalli, S.; Presser, N.; Kitsopoulos, T.; Gordon, R. J. *J. Chem. Phys.* **1990**, *92*, 7382−7393.
(41) Garton, D. J.; Minton, T. K.; Maiti, B.; Troya, D.; Schatz, G. C. *J. Chem. Phys.* **2003**, *118*, 1585−1588.
(42) Maiti, B.; Schatz, G. C. *J. Chem. Phys.* **2003**, *119*, 12360−12371.
(43) Braunstein, M.; Adler-Golden, S.; Maiti, B.; Schatz, G. C. *J. Chem. Phys.* **2004**, *121*, 4316−4323.
(44) Balakrishnan, N. *J. Chem. Phys.* **2003**, *119*, 195−199.
(45) Press: W.; Flannery, B.; Teukolsky, S.; Vetterling, W. *Numerical Recipes: the Art of Scientific Computing*, 2nd ed.; Cambridge University Press: Cambridge, 1992.
(46) Leforestier, C.; Bisselling, R. H.; Cerjan, C.; Feit, M. D.; Friesner, R.; Guldberg, A.; Hammerich, A.; Jolicard, G.; Karrlein, W.; Meyer, H. D.; Lipkin, N.; Roncero, O.; Kosloff, R. *J. Comput. Phys.* **1991**, *94*, 59−80.
(47) Feit, M. D.; Fleck, J. A.; Steiger, A. *J. Comput. Phys.* **1982**, *47*, 412.
(48) Light, J. C.; Hamilton, I. P.; Lill, J. V. *J. Chem. Phys.* **1985**, *82*, 1400.